GEORGIA INSTITUTE OF TECHNOLOGY
OFFICE OF CONTRACT ADMINISTRATION

SPONSORED PROJECT INITIATION

Date: 10/10/77

Project Title: "Study of Gas Transfer Characteristics of Hydraulic Jumps."

Project No: E-20-626

Project Director: Dr. J. R. Wallace

Sponsor: U. S. Army Waterways Experiment Station, Corps of Engineers

Agreement Period: From 9/28/77 Until ~~9/27/78~~ 26 apr 79 (Contract Term)

Type Agreement: Contract No. DACW39-77-C-0079

Amount: $17,740

Reports Required: Quarterly Progress Reports, Final Report

Sponsor Contact Person (s):

Technical Matters	Contractual Matters (thru OCA)
Mr. Darrell G. Fontane Structures Division, Hydraulics Lab USAE Waterways Experiment Station, CE Vicksburg, MS 39180	A. J. Breithaupt Procurement & Supply Officer U. S. Army Waterways Experiment Station Corps of Engineers Vicksburg, MS 39180

Defense Priority Rating: N/A

Assigned to: Civil Engineering (School/Laboratory)

COPIES TO:

- Project Director
- Division Chief (EES)
- School/Laboratory Director
- Dean/Director—EES
- Accounting Office
- Procurement Office
- Security Coordinator (OCA)
- Reports Coordinator (OCA)
- Library, Technical Reports Section
- Office of Computing Services
- Director, Physical Plant
- EES Information Office
- Project File (OCA)
- Project Code (GTRI)
- Other ____________

CA-3 (3/76)

GEORGIA INSTITUTE OF TECHNOLOGY
OFFICE OF CONTRACT ADMINISTRATION

SPONSORED PROJECT TERMINATION

Date: August 2, 1979

Project Title: "Study of Gas Transfer Characteristics of Hydraulic Jumps."

Project No: E-20-626

Project Director: Dr. J.R. Wallace

Sponsor:

Effective Termination Date: 4/26/79

Clearance of Accounting Charges: 4/26/79

Grant/Contract Closeout Actions Remaining:

- _ Final Invoice and Closing Documents
- _ Final Fiscal Report
- _ Final Report of Inventions
- XX Govt. Property Inventory & Related Certificate
- _ Classified Material Certificate
- _ Other ____________________

Assigned to: Civil Engineering (School/Laboratory)

COPIES TO:

Project Director
Division Chief (EES)
School/Laboratory Director
Dean/Director—EES
Accounting Office
Procurement Office
Security Coordinator (OCA)
√Reports Coordinator (OCA)

Library, Technical Reports Section
EES Information Office
Project File (OCA)
Project Code (GTRI)
Other ____________________

CA–4 (1/79)

E-20-626

FINAL REPORT

PROJECT E20-626

MODELING GAS TRANSFER IN HYDRAULIC JUMPS

By

Steven C. Wilhelms

James R. Wallace

Prepared for

U. S. ARMY ENGINEER WATERWAYS EXPERIMENT STATION VICKSBURG, MISS.

April 1979

GEORGIA INSTITUTE OF TECHNOLOGY

SCHOOL OF CIVIL ENGINEERING

ATLANTA, GEORGIA 30332

1979

Modeling Gas Transfer in Hydraulic Jumps

By Steven C. Wilhelms

and

James R. Wallace

Preface

This investigation was conducted at the Georgia Institute of Technology, School of Civil Engineering from October 1977 to September 1978 and was funded by the U. S. Army Engineer Waterways Experiment Station. The investigation was under the supervision of Dr. J. R. Wallace, Associate Professor of Civil Engineering. In partial fulfillment of the requirements for the Master of Science in Civil Engineering, Mr. Steven C. Wilhelms conducted the experiments. Also assisting in the testing and analysis were Messrs. G. P. Utterbeck, L. M. Rennell, P. J. Mitchell, A. C. Waite and Mrs. S. M. Wilhelms. This report was prepared by Messrs. Wilhelms and Wallace.

Table of Contents

CONVERSION FACTORS, U. S. CUSTOMARY TO METRIC (SI)
UNITS OF MEASUREMENT

U. S. Customary units of measurement used in this report can be converted to metric units as follows:

Multiply	By	To Obtain
Feet	0.3048	Metres
Cubic feet per second (cfs)	0.0283168	cubic metres per second (cms)
Inches	0.3937	centimetres
Feet per second (fps)	0.3048	metres per second (mps)

PART I: INTRODUCTION

Background

1. Many kinds of aquatic life cannot survive without an adequate dissolved oxygen (DO) concentration in their watery environment. These organisms depend on the natural diffusion processes which replenish the DO as it is used. Direct absorption of atmospheric oxygen into water, termed reaeration, is one such process. The rate of reaeration is of utmost importance to underwater ecology since the DO must be replenished at a rate that is, on the average, at least as great as the rate at which it is being used.

2. Reaeration can be considered as two processes acting together, molecular diffusion and turbulent convection. Molecular diffusion is very slow compared to turbulent convection. Thus, in most natural systems, turbulent convection is the dominant process determining the rate of reaeration.

3. Physical mixing, or turbulence, is a very complex process which is influenced by the physical characteristics of the fluid in which the mixing occurs, the geometry of the system where the fluid is located, and the forces acting on the fluid. The complex combination of these factors precludes the accurate measurement of fluid turbulence. Since turbulence cannot be accurately measured, it is not possible to describe reaeration rates directly in terms of turbulence.

4. The Federal Water Pollution Control Administration developed a procedure for accurately evaluating stream reaeration

capacity. A gaseous tracer,[1] which was the basis for the procedure, was tested in field measurements[2] of stream reaeration. The development of the gaseous tracer technique marked a significant advance in the study of the reaeration process. The technique has been successfully applied to numerous streams[3] and is becoming accepted as the best method available for determining stream reaeration rates.[4]

5. There are still many unanswered questions concerning reaeration or gas-transfer. All of the studies mentioned have been on streams flowing in natural channels leaving essentially untouched the subject of reaeration in man-made structures such as stilling basins below dams, power house tailraces, or other reservoir outlet structures. The importance of understanding gas-transfer characteristics of these systems lies in the designers' ability to build into these structures feature which promote gas-transfer as the flow passes through and downstream of the structures.

6. By using the tracer technique the actual structure could, in many cases, be tested and its gas-transfer characteristic determined. But this can be very costly and not always possible. Evaluating different designs in a prototype would be prohibitively expensive. If a structure is in the planning stage, a prototype does not exist.

7. Because of these problems it would be advantageous to test a hydraulic model to determine the model's gas-transfer characteristics under different designs and thereby estimate

the gas-transfer in the prototype. At present, however, scaling laws that would permit the prediction of prototype gas transfer are unknown.

Objective

8. The objective of this study was to use the gaseous tracer to determine the gas-transfer characteristics of hydraulics jumps and make initial estimates of scaling laws that would provide a basis for transfering reaeration rates from model to prototype.

Scope

9. The gas-transfer characteristics of various hydraulic jumps (different Froude numbers) were determined. The jumps were modeled according to Froudian criterion and reaeration characteristics determined. The "prototype" characteristics were compared to the "model" characteristics to analyze the effect of "scale".

PART II: METHODOLOGY

Tracer Technique

10. The gaseous tracer method utilized in this study is based on two tracers simultaneously and continuously injected into the flow at a steady rate. Krypton-85 (Kr-85), as a dissolved gas, was the tracer for dissolved oxygen. Rhodamine-WT flourescent dye was the tracer for dispersion.

11. To understand the tracer method, the equivalence of two processes must be made clear. The absorption of atmospheric gases (oxygen being of primary interest) into the water or the desorption of tracer gas from water to the atmosphere are equi-

valent. In either case the driving force for gas transfer is the difference between the partial pressures of the gas in the atmosphere and in the water. For oxygen, a measure of the strength of the force, called "saturation deficit," D_{ox}, is the difference between the oxygen concentration at saturation, C_s, and the concentration of oxygen, C, which actually exists in the water. Thus,

$$D_{ox} = (C_s - C)_{ox} \tag{1}$$

12. As long as the concentration of oxygen in the water is less than the saturation concentration, there will be a net movement of oxygen from the atmosphere to the water. This process can be represented by

$$\frac{dD}{dt} = -K_{ox}D \tag{2}$$

where t is time and K_{ox} is a proportionality constant referred to as the "reaeration rate coefficient." This equation simply states that the rate of change of the saturation deficit at any time is proportional to the deficit at that time, or, the greater the deficit, the greater the rate of reaeration. The magnitude of the proportionality constant, K_{ox}, is dependent particularly upon the intensity of turbulent mixing in the system.

13. If there were no factors other than turbulent mixing

affecting the oxygen concentration, integrating equation 2 would provide a means for determining the proportionality constant, K_{ox}, through the relationship

$$D = D_o \exp(-K_{ox} t) \tag{3}$$

where

D_o = Saturation deficit at some initial time, (t = o)

D = Saturation deficit at some later time t

There are many chemical and biological processes which affect DO in natural systems and, therefore, it is important to use an inert gas as the tracer so that no gas is lost through such processes.

14. The desorption process of krypton from the water is equivalent to the absorption process of oxygen from the atmosphere. The driving force in the desorption of the tracer gas is the difference between the partial pressure of the krypton in the water and the partial pressure of the krypton in the atmosphere. For all practical purposes, the concentration of krypton in the atmosphere is zero. A measure of the strength of the force causing gas loss is simply the concentration of tracer gas in the water. This process can be represented by

$$C = C_o \exp(-K_{kr} t) \tag{4}$$

where

C_o = concentration of kr-85 at some initial time (t = o)

C = concentration of kr-85 remaining in the water at some later time, t

Since krypton gas is inert, it is not subject to the chemical and biological processes which affect oxygen. This fact makes it possible to compute, through Equation 4, a gas exchange coefficient for krypton, K_{kr}, which reflects only the turbulent mixing process and direct physical gas transfer.

15. It has been shown that the ratio of exchange coefficients for these two gases is equal to a constant,[1] that is,

$$\frac{K_{kr}}{K_{ox}} = 0.83 \tag{5}$$

where

K_{kr} = exchange coefficient for krypton

K_{ox} = exchange coefficient for oxygen

This relationship is not affected by temperature (within the range of interest), degree of turbulent mixing, or the direction of gas transfer. This makes possible the calculation of K_{kr} from equation 4 in the form

$$\frac{C_B}{C_A} = \exp(-K_{kr}t) \tag{6}$$

where

C_A, C_B = krypton gas concentration at A and B

t = time-of-travel from A to B (time needed for a drop of water to flow from A to B)

17. However, since dilution and dispersion are present, they must be taken into account. Even if it were possible, direct measurement of dispersion and dilution is not necessary. A correction which accounts for dispersion and dilution may be applied to equation 6 by using the flourescent dye concentrations. The flourescent dye, in solution in the tracer mixture, is released simultaneously with the krypton gas. The dye concentration decreases from point A to point B since it is subjected to the dispersion and dilution of the reach. Thus, it provides a measure of the turbulent mixing and dilution. With flow conditions such as those in these tests, the amount of dye which might be adsorbed on the flume or otherwise lost was considered insignificant. Because the tracers are injected simultaneously, the krypton-85 undergoes the same dispersion and dilution as the dye.

18. The observed concentrations of the dye provide a correction for the effects of turbulent mixing and dilution which can be applied to the krypton-85 concentration. The krypton exchange coefficient, K_{kr}, can be calculated by

$$\frac{\left(\frac{C_{kr}}{C_D}\right)_B}{\left(\frac{C_{kr}}{C_D}\right)_A} = \exp(-K_{kr}t) \tag{7}$$

where

$\left(\frac{C_{kr}}{C_D}\right)_A, \left(\frac{C_{kr}}{C_D}\right)_B$ = Ratios of krypton concentration to dye concentration at points A and B

t = time of flow from A to B

19. In the present study the two tracers are mixed together and are injected simultaneously. Samples taken from the flow at stations A and B are analyzed in a liquid scintillation counter for krypton content and in a fluorometer for dye content. The travel time is obtained from brine (conductivity) tests described in paragraph 32. The observed data thus permit the calculation of the krypton exchange coefficient, K_{kr}, and subsequent determination of K_{ox} for the reach AB.

Testing Facilities

Description

20. The flume used in this study was glass-walled and 1.25 ft. wide with a range of flow up to 0.6 cfs. (Figure 1) A vertical sluice gate was used to control the depth of water in the headbay, thus controlling the velocity of the flow upstream of the hydraulic jump. A tailgate varied the tailwater depth which caused the jump to position itself longitudinally in the

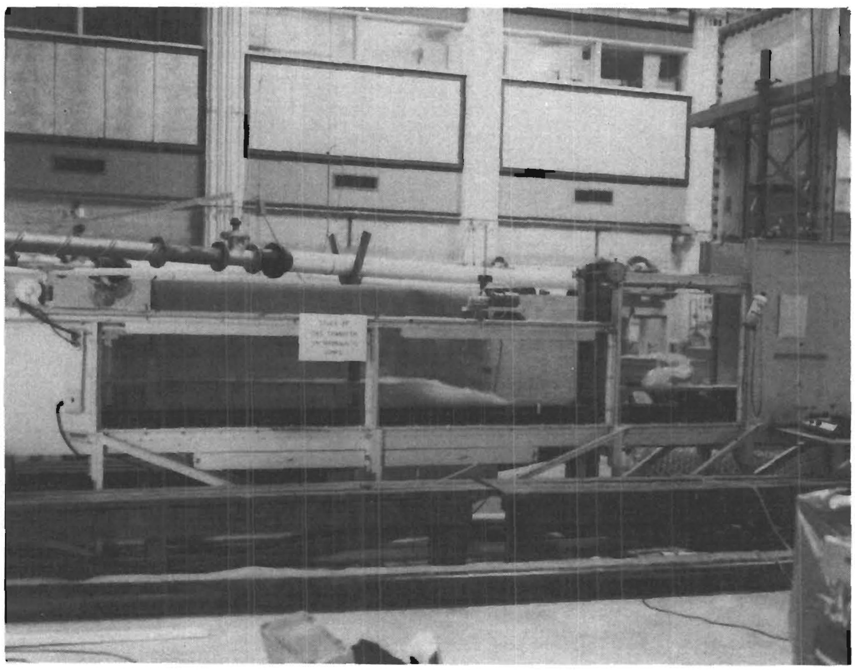

FIGURE 1: TESTING FACILITIES

flume. The flow in the flume was determined with a calibrated elbow meter and manometer.

21. A pitot-static tube was used to determine the velocity head of the supercritical flow upstream of the jump. The velocity was computed from the velocity head. A simple point gage was used to determine the depth of flow upstream of the jump.

22. Water samples were collected at two depths using two Masterflex tubing pumps. Both pumps were driven by the same motor to assure that their pumping rates were the same. The sample intakes were 1/4" stainless steel tubes connected to the tygon tubing leading to the pumps (Figure 2). Care was exercised to obtain identical length of tubing in the sampling system to assure that samples would be taken simultaneously.

23. The radioactive dose (krypton-85 and dye) was injected continuously into the headbay with a precision syringe pump (Figure 3). The injection location was just upstream of a Venturi section placed in the headbay (Figure 4). A 1/8" diameter stainless steel tube with three small holes (0.0156 inch diameter) was used as a manifold to distribute the dose across the width of flow. The dosed water then flowed through a confined section to the sluice gate. This prevented gas loss upstream of the sluice gate.

24. The entire flume was covered and a blower placed at the downstream end of the flume which allowed the air space above the flowing water to be exhausted to the atmosphere outside the lab. This prevented escape of radioactive gas into the laboratory.

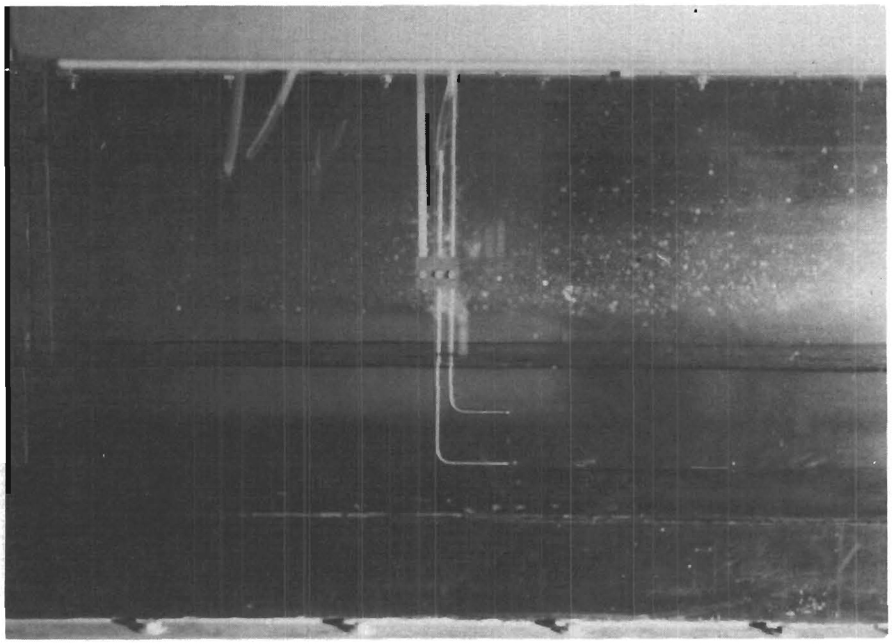

FIGURE 2: SAMPLER INTAKES

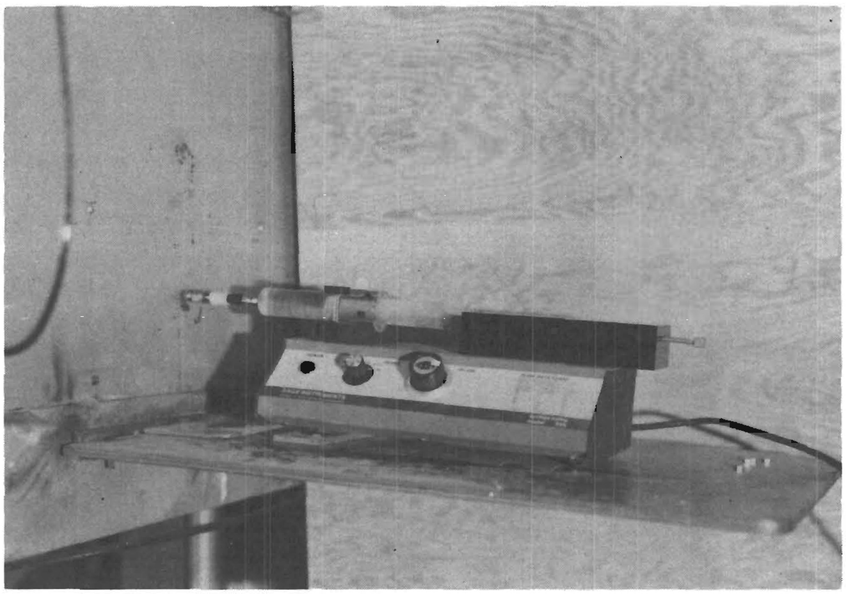

FIGURE 3: PRECISION SYRINGE PUMP

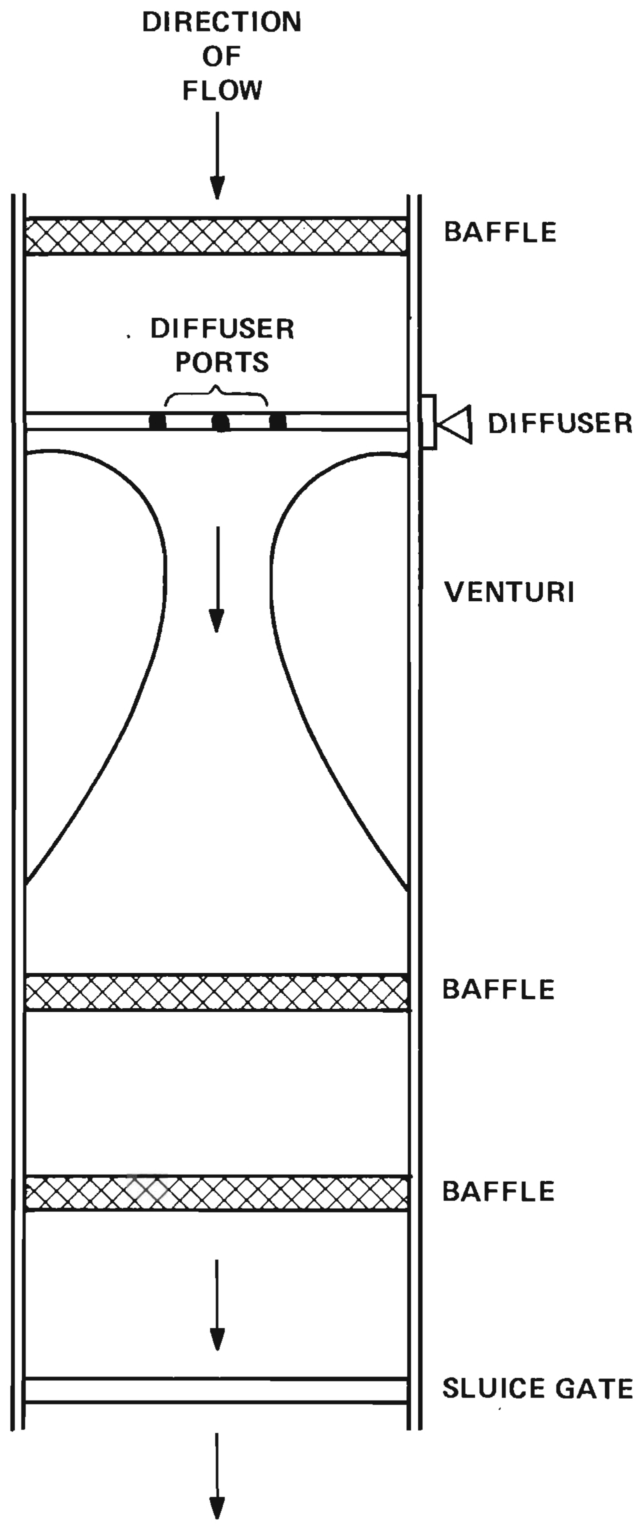

FIGURE 4: VENTURI AND DIFFUSER UPSTREAM OF SLUICE GATE

Hydraulic Scaling Criteria

25. In open channel or free surface flow, the predominant forces are inertia and gravity. In modeling such systems, the Froude number, which is a dimensionless ratio of inertial forces to gravitational forces, is used. The Froude number of the prototype is set equal to the Froude number of the model, thus determining the scale relationships of system dimensions.

26. In this study the following scales were used:

Dimension	Ratio	Scale Relation
Length	$L_r = \frac{L_m}{L_p}$	1:1.460
Time	$T_r = L_r^{1/2}$	1:1.208
Flow	$Q_r = L_r^{5/2}$	1:2.576
Velocity	$V_r = L_r^{1/2}$	1:1.208

Measurements of discharge, velocity, and depth can be transferred quantitatively from model to prototype with these relationships.

Hydraulic Model

27. Modeling a hydraulic jump in a rectangular flume was considered a two-dimensional problem and variations in a transverse direction were not considered. Therefore by scaling the vertical and longitudinal dimensions according to the relationshps described in paragraph 26 and scaling the discharge per unit

width, the jump was "modeled" without regard to width.

28. The total flow through the flume under the "prototype" condition was

$$Q_p(\text{total}) = 0.578 \text{ cfs}$$

Thus the unit discharge for the prototype was

$$q_p = \frac{Q_p(\text{total})}{W} = \frac{0.578}{1.25} = 0.462 \text{ cfs}$$

where

$$w = \text{flume width, ft.}$$

The "modeled" unit discharge, q_m, was

$$q_m = (q_p)Q_r = 0.462(0.3883) = 0.179 \text{ cfs}$$

where

Q_r = Froudian scale relationshp for discharge (para 26)

However, the unit width for the modeled flow is scaled down with the Froudian scale relation for length, L_r. Thus the 0.179 cfs per unit width actually flows in

$$L_r(L_p) = \frac{1}{1.46}(1.0) = 0.685 \text{ ft.}$$

where

L_p = unit width in the prototype which was 1.0 ft.

The modeled flow per foot of flume width, q', was

$$q' = (0.179)\frac{1}{0.685} = 0.261 \text{ cfs}$$

Total flow in the flume for the "model" condition was

$$Q_m(\text{total}) = (q')W = 0.261(1.25) = 0.327 \text{ cfs}$$

PART III: TESTING

Hydraulic Conditions

29. Several kinds of hydraulic jumps were tested. The type of jump depended on the Froude number. Hydraulic jumps have been classified[5] as undulating, F=1 - 1.7; weak, F = 1.7 - 2.5; oscillating, F = 2.5 - 4.5; or steady with a range of Froude numbers from 4.5 to 9.0. Hydraulic jumps with Froude numbers in these ranges were studied. Figure 5 shows a hydraulic jump with F = 9.3. Figures, 6, 7, 8 and 9 show jumps with Froude numbers of 5.8, 3.3, 2.4, and 1.8, respectively. These figures illustrate the different jumps tested and give an impression of the different levels of turbulent mixing involved.

Procedure

30. The particular flow condition to be tested was established and allowed to stabilize. The velocity upstream of the jump was determined along with the depth of flow. The Froude number was computed from these data by

$$F = \frac{V}{(gd)^{1/2}}$$

where

F = Froude number

V = velocity upstream of the jump, ft./sec.

d = depth upstream of the jump, ft.

g = gravitational acceleration = 32.2 ft./sec.^{2}

The depth of flow downstream was computed from the equation[4]

$$\frac{Y_2}{Y_1} = 1/2 \left((1 + 8F^2)^{\frac{1}{2}} - 1 \right)$$

where

Y_2 = downstream depth, ft.

Y_1 = upstream depth, ft.

31. The jump length, L, was determined from an empirical relationshp (Ref 4, p 398) of $\frac{L}{Y_2}$ and F. The sampling locations were established by moving downstream from the leading edge of the jump. For most tests, samples were taken at the leading edge (Figure 5) and at distances of one, two, and three jump lengths from the leading edge, stations A, B, C, and D, respectively.

32. Time of flow between stations was determined using conductivity probes and a salt brine. The conductivity probes were placed at the leading edge of the jump and at one of the

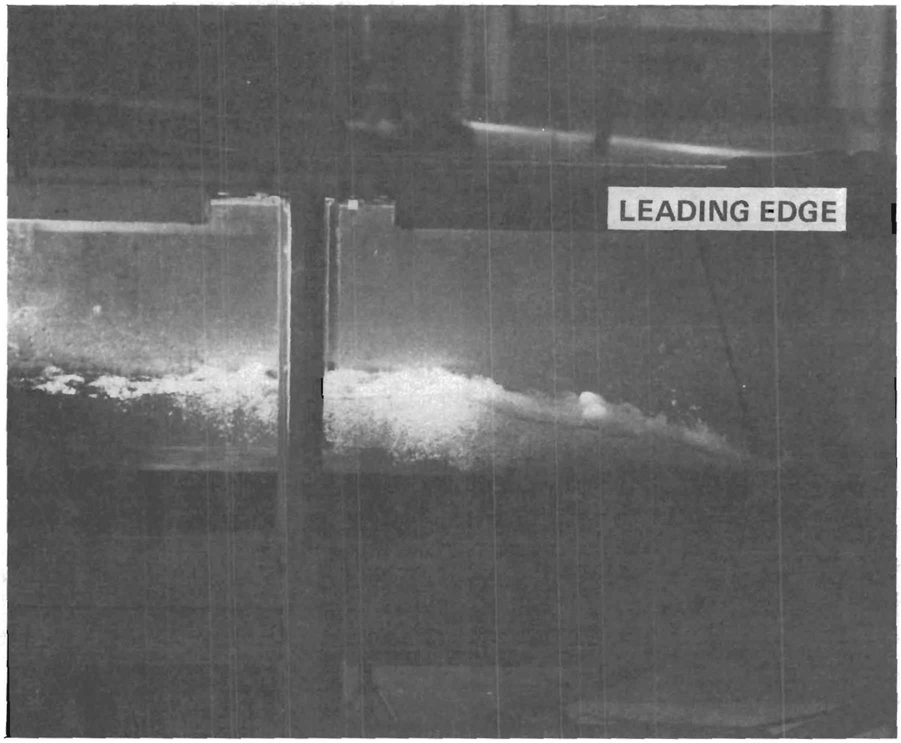

FIGURE 5: HYDRAULIC JUMP, F = 9.3

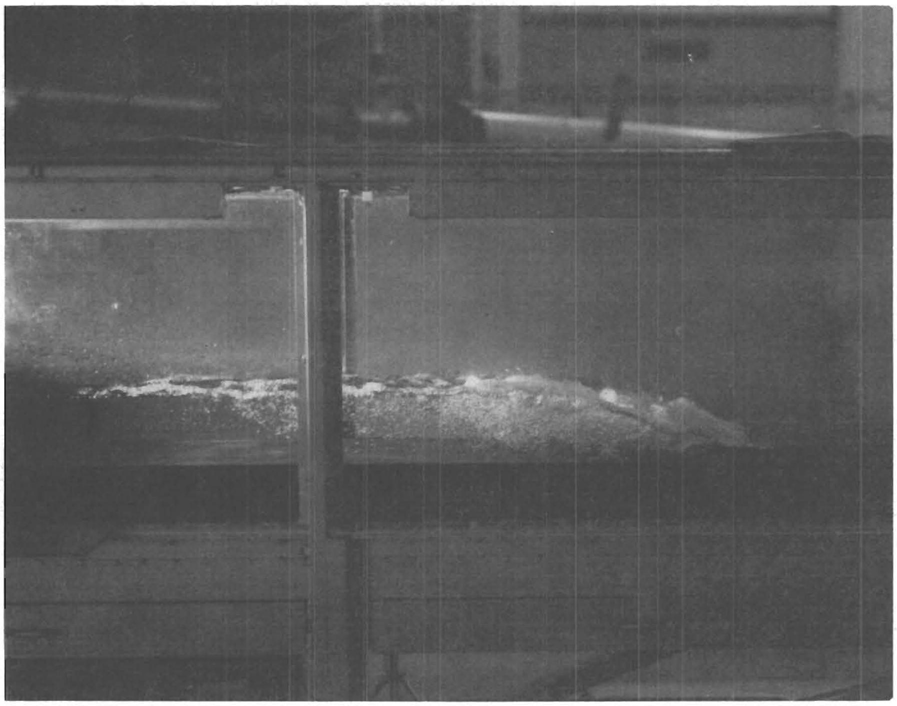

FIGURE 6: HYDRAULIC JUMP, F = 5.9

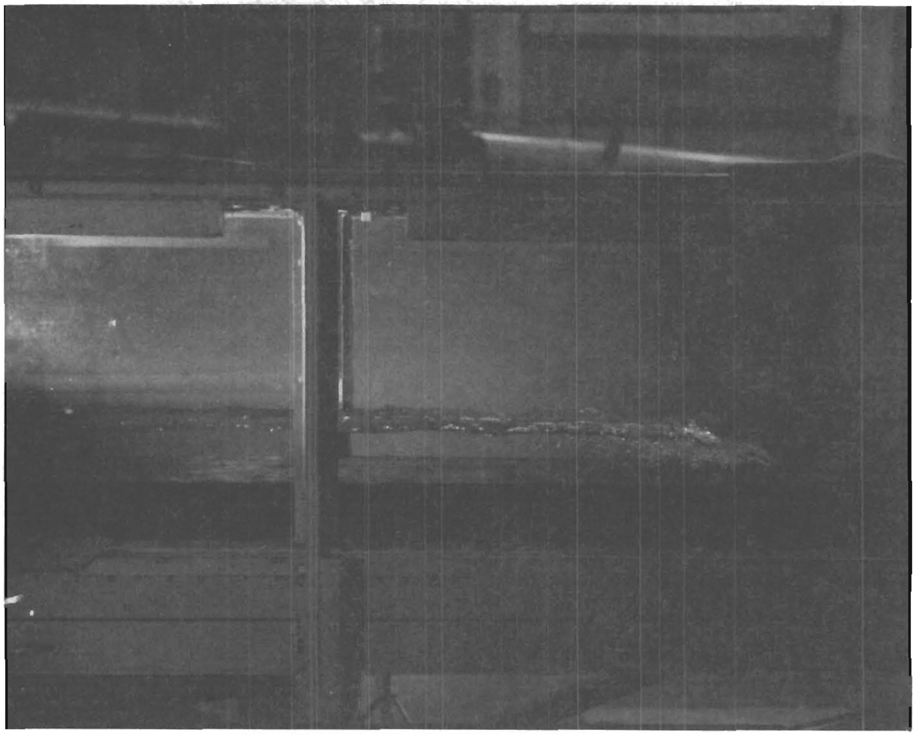

FIGURE 7: HYDRAULIC JUMP, F = 3.3

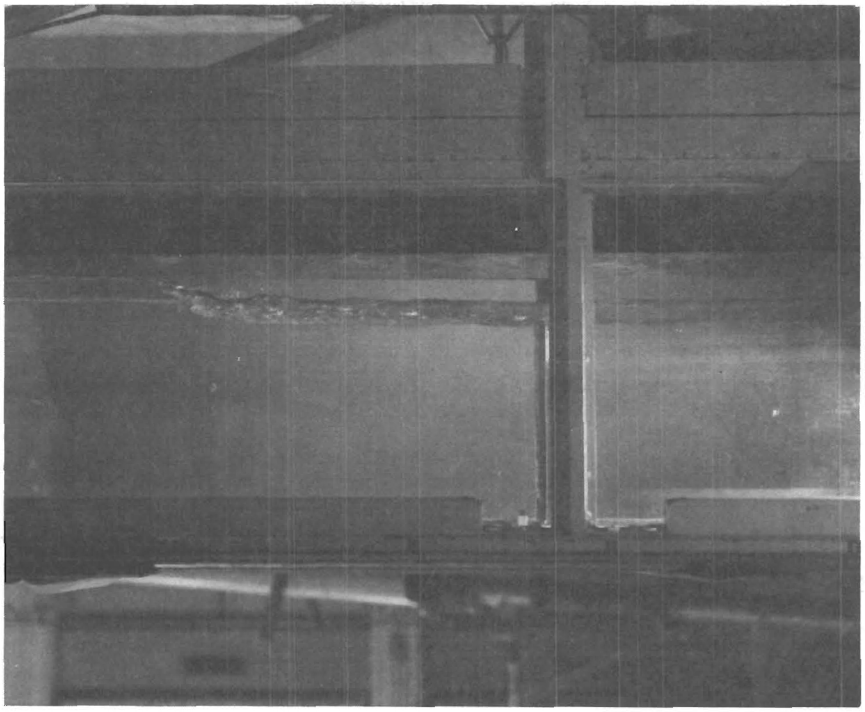

FIGURE 8: HYDRAULIC JUMP, F = 2.4

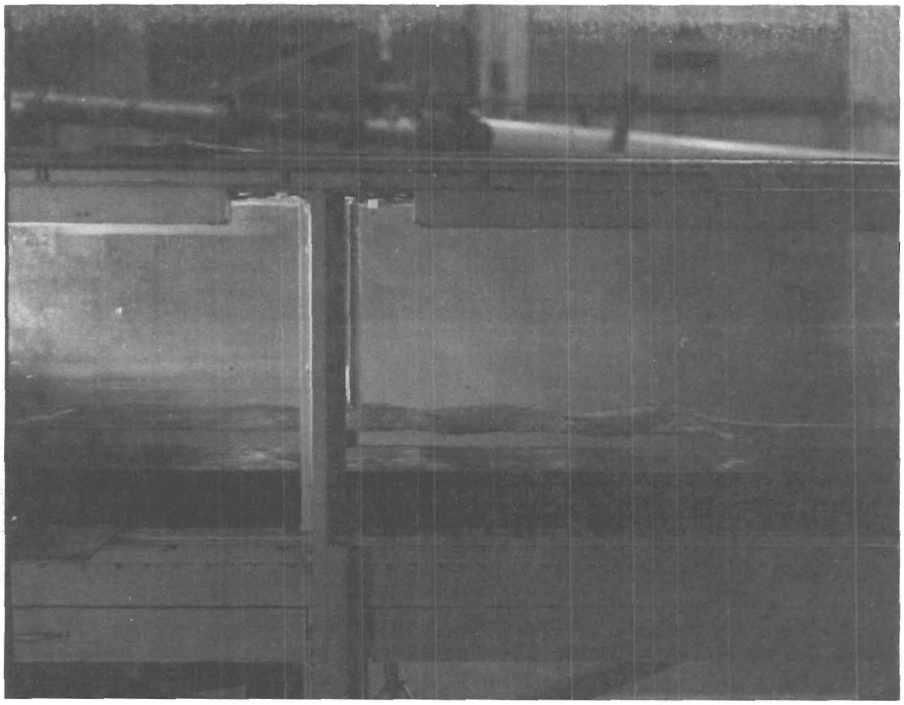

FIGURE 9: HYDRAULIC JUMP, F = 1.8

other specified multiples of the jump length. An "instantaneous" dose of brine . introduced upstream of the jump. The conductivity of the water increased and then decreased as the cloud of brine passed the sampling locations.

33. The passing of the brine cloud was recorded on a high speed strip chart recorder (Figure 10). The lapse time between peaks on the recording was the time of flow between the leading edge and the station being tested. This test was repeated several times at each location to determine a mean travel time.

34. To efficiently locate sampling stations during a test the following scheme was devised. The sampling pumps were mounted on a carriage which could be rolled along the flume longitudinally. The sampling system (pumps and carriage) was positioned at the leading edge of the jump (Figure 11). A small c-clamp chocked the rollers to prevent movement of the carriage. Other clamps were placed at multiples of the jump length downstream. When sampling was completed at one station, the clamp chocking the carriage was removed, and the carriage rolled downstream to the next clamp which positioned the sampling system at the correct location.

35. Samples were drawn from the quarter-depths of the tail-water, i.e., at 1/4 and 3/4 of the tailwater depth to determine if stratified flow existed in the jump. The sample bottles were equipped with plastic tubing reservoirs (Figure 12) which provided the extra water needed to assure full sample bottles when the tygon tubes were withdrawn.

36. The dye and krypton tracers were injected simultaneously. The tracer mixture was provided in a sealed capped bottle. The

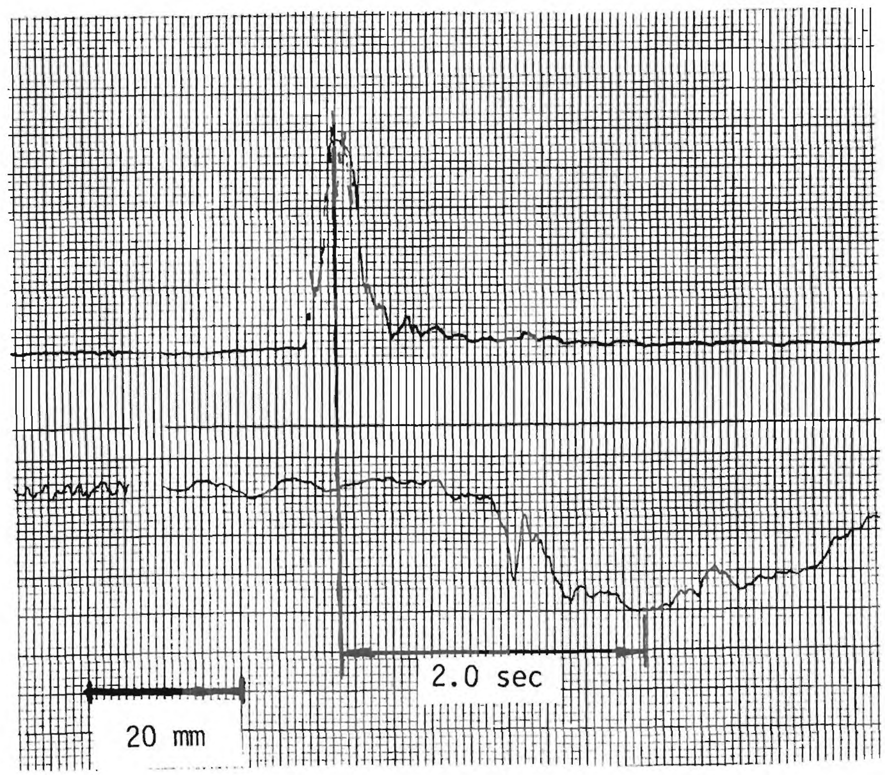

FIGURE 10: STRIP CHART RECORDING OF CONDUCTIVITY AS BRINE DOSE PASSED STATIONS, F = 9.4, Chart Speed 20 mm/sec, 1 jump length from leading edge.

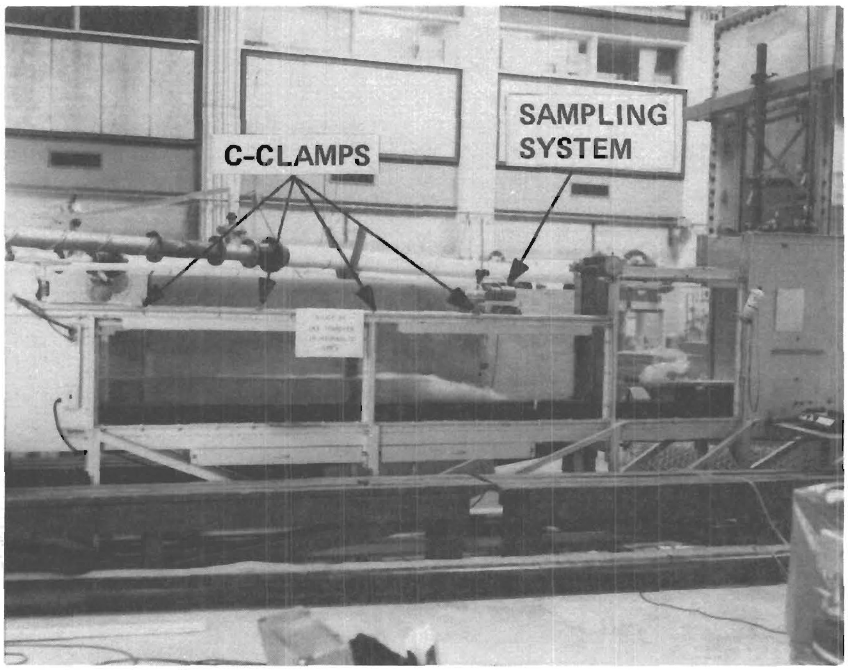

FIGURE 11: SAMPLING STATION LOCATION

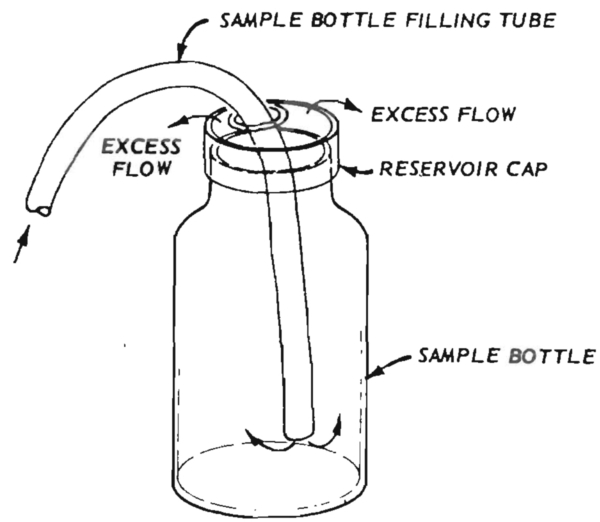

FIGURE 12: SAMPLE BOTTLE AND RESERVOIR CAP

mixture was transferred to a 50 cc glass syringe by using a second syringe to force the dose from the dose bottle into the 50 cc syringe (Figure 13). The 50 cc injection syringe was fitted with a 3-inch long needle which extended well down into the bottle. The 50 cc syringe's needle and a short needle attached to a 100 cc syringe were passed through a rubber stopper. The rubber stopper was fitted into the mouth of the dose bottle (Figure 14). The 100 cc syringe was plunged forcing the tracers into the 50 cc syringe. This operation successfully prevented krypton loss from the mixture since no air or air bubbles came in contact with the mixture.

37. When a test was completed, the sample bottles were capped and taped shut with plastic electrical tape. They were placed in water for temperature stability and transported to the laboratory for analysis.

Analysis

38. As has been stated, the travel time between the sampling stations was determined with conductivity tests. The lapse time from peak conductivity upstream to peak conductivity downstream was the time of travel between the sampling stations.

39. The water samples withdrawn from the flume during each test were prepared for analysis by the method described by Cohen, et.al.[6] The krypton-85 concentrations were determined in a liquid scintillation counter. Three replicates of each sample were prepared and cycled through three counting sequences to reduce the effect of any laboratory or counting errors. A

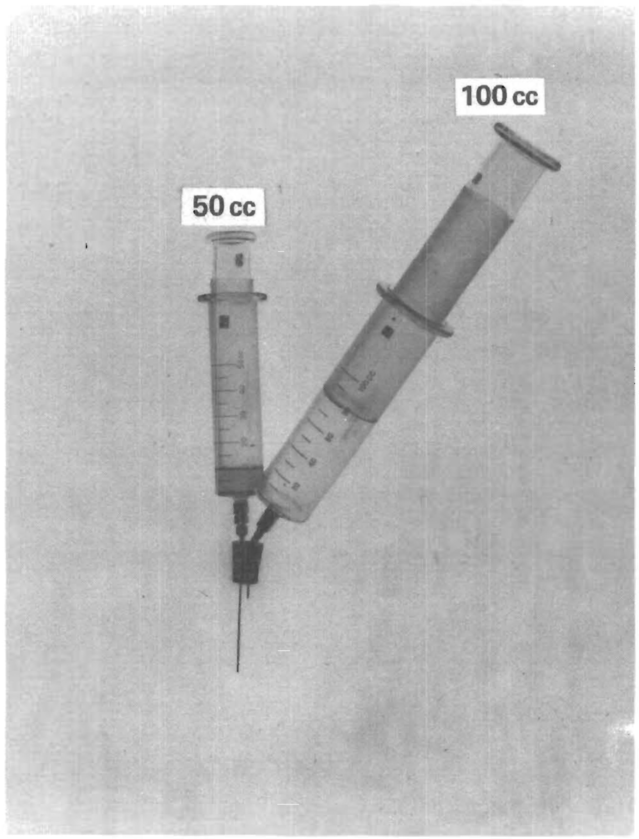

FIGURE 13: SYRINGE SET-UP

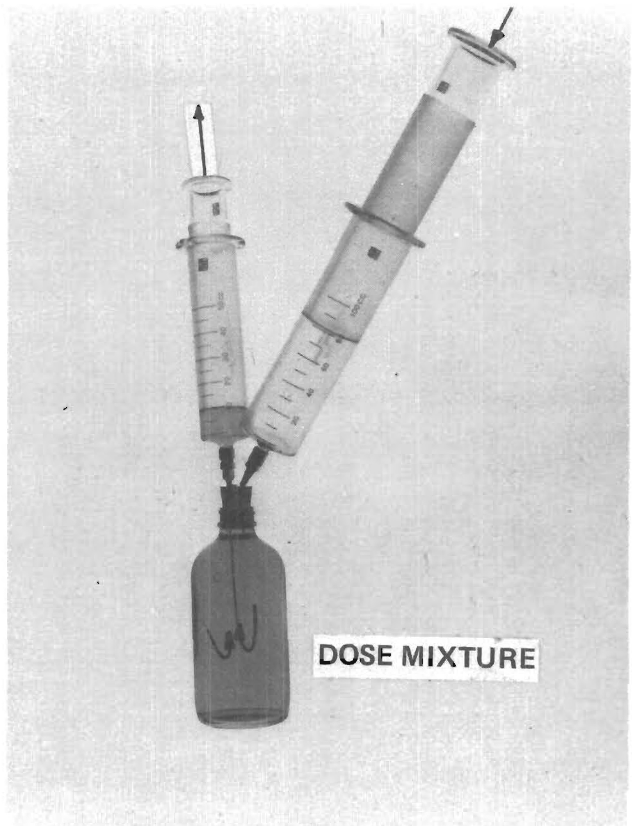

FIGURE 14: DOSE TRANSFER

fluorometer was used to determine the dye concentrations of the samples.

40. The ratios of krypton-85 to dye were plotted on a semilog coordinate system with time as the abscissa. The slope of the line was the krypton-85 exchange coefficient for the particular jump. By applying equation 7, the exchange coefficient for oxygen was determined. Applying a temperature correction,[7]

$$K_{ox}^{20} = K_{ox}^{T} 1.022^{(20-T)} \tag{8}$$

where

K_{ox}^{20}, K_{ox}^{T} = oxygen exchange coefficients at temperatures of 20°C and T°C

the exchange coefficient for oxygen at 20°C was computed.

PART IV: RESULTS

41. Appendix 1A presents tables of the krypton-to-dye ratios for the "prototype" jumps tested. Appendix 1B presents tables of the krypton-to-dye ratios of the "model" jumps tested. Other pertinent hydraulic data are presented.

42. Appendix 2A shows the graphs of krypton-to-dye ratios versus time for the "prototype" tests. Appendix 2B shows graphs of the ratios versus time for the "model" tests. The spread in the observed ratios from highest to the lowest are indicated. The lines connect the mean ratios.

43. Consider the data from Appendix 1A, Test 1. The gas fraction remaining in the water at station C was

$$\frac{88.23}{104.70} = 0.843$$

The gas fraction lost to the atmosphere was

$$1.000 - 0.843 = 0.157$$

That is, 15.7 per cent of the gas in the water at station A was lost to the atmosphere by the time the flow reached station C, one jump length from A. Similar computations were made for the other tests. By applying equations 7, 5, then 8, the exchange coefficients for oxygen, 20°C, K_{ox}^{20}, was obtained.

44. Table 1 presents the observed gas loss and oxygen exchange coefficients computed from the data for the flume segment extending from the leading edge of the jump to one jump length downstream.

Table 1

Exchange Coefficients for One Jump Length from A, "prototype"

Test	F	% gas loss	Travel time-sec	K^T_{kr} /sec	K^{20}_{ox} /sec
1*	9.5	15.7	1.928	.089	.098
2*	9.8	17.5	1.620	.119	.129
3*	9.4	17.0	1.29	.145	.163
4	5.95	11.7	1.37	.091	.102
5	5.85	10.0	1.32	.080	.090
6	3.27	4.3	0.95	.046	.052
7	3.28	1.3	0.99	.014	.015
8	2.72	1.8	0.94	.019	.018
9	2.34	2.0	0.71	.028	.026
10	1.84	NA	0.47	NA	NA

* These were computed from data at stations A and C since station B is only 1/2 jump length from A.

Table 2

Exchange Coefficients for One Jump Length from A, "model"

Test	F	% gas loss	time-sec	K^T_{kr} /sec	K^{20}_{ox} /sec
1	9.30	12.4	1.65	.080	.092
2	9.40	13.2	1.51	.094	.107
3	6.20	4.9	1.49	.034	.039
4	6.19	7.1	1.46	.050	.058
5	3.7	NA	1.00	NA	NA

45. The data presented in tables 1 and 2 indicate that the reaeration rate coefficients, K_{ox}^{20}, vary greatly for replicate tests. This is a direct result of the large variability in measured travel time as illustrated in figure 15. There was extreme variation (from 1.3 to 1.9 seconds) in observed travel times for the prototype jumps with $F \geq 9.0$. A subsequent travel time test, replicating test 3, F = 9.4, indicated that the time of flow was 1.81 seconds. This leads to the conclusion that time-of-flow measurement error was so great that it prevented using K_{ox} for scaling analysis. Instead, gas loss was evaluated.

46. Figure 16 shows percent gas loss versus Froude number on a semilog coordinate system for the model and prototype jumps. The gas loss in the "model" hydraulic jump was less than the gas loss in the "prototype."

PART V: CONCLUSIONS

47. The tracer technique was a useful tool in determining the gas transfer occurring in hydraulic jumps. There appears to be a lower limit below which gas loss is undetectable. For the "prototype" and "model" jumps tested this limit was approximately at Froude numbers of 2.0 and 3.7, respectively. In the jumps tested, gas transfer occurred in the first jump length downstream of the leading edge. Thereafter gas loss was undetectable.

48. The observed travel times in these tests had the greatest variability of all the observed parameters. Other methods of measuring travel time must be devised or the travel time must be

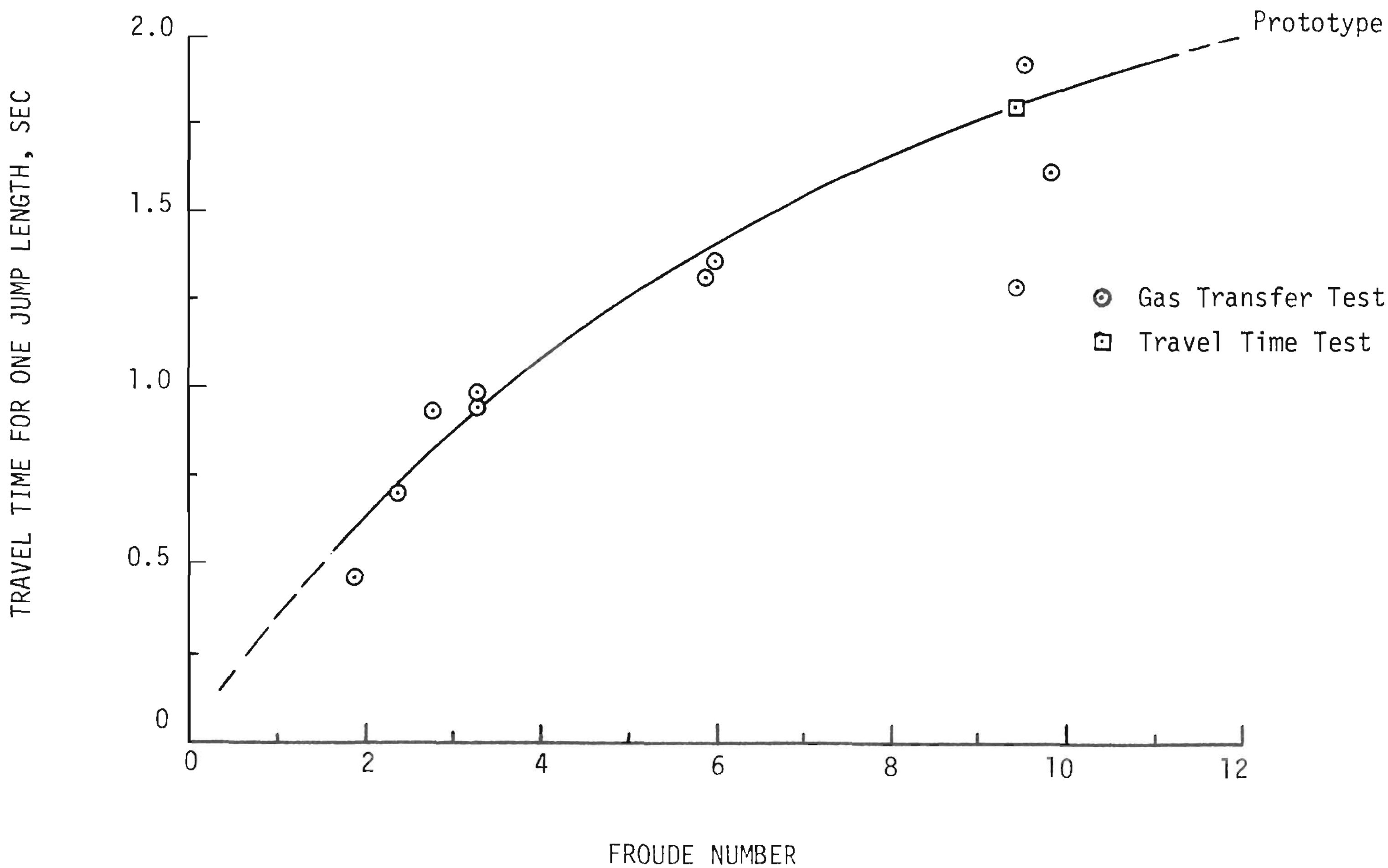

FIGURE 15: TRAVEL TIME VERSUS NUMBER-PROTOTYPE JUMP

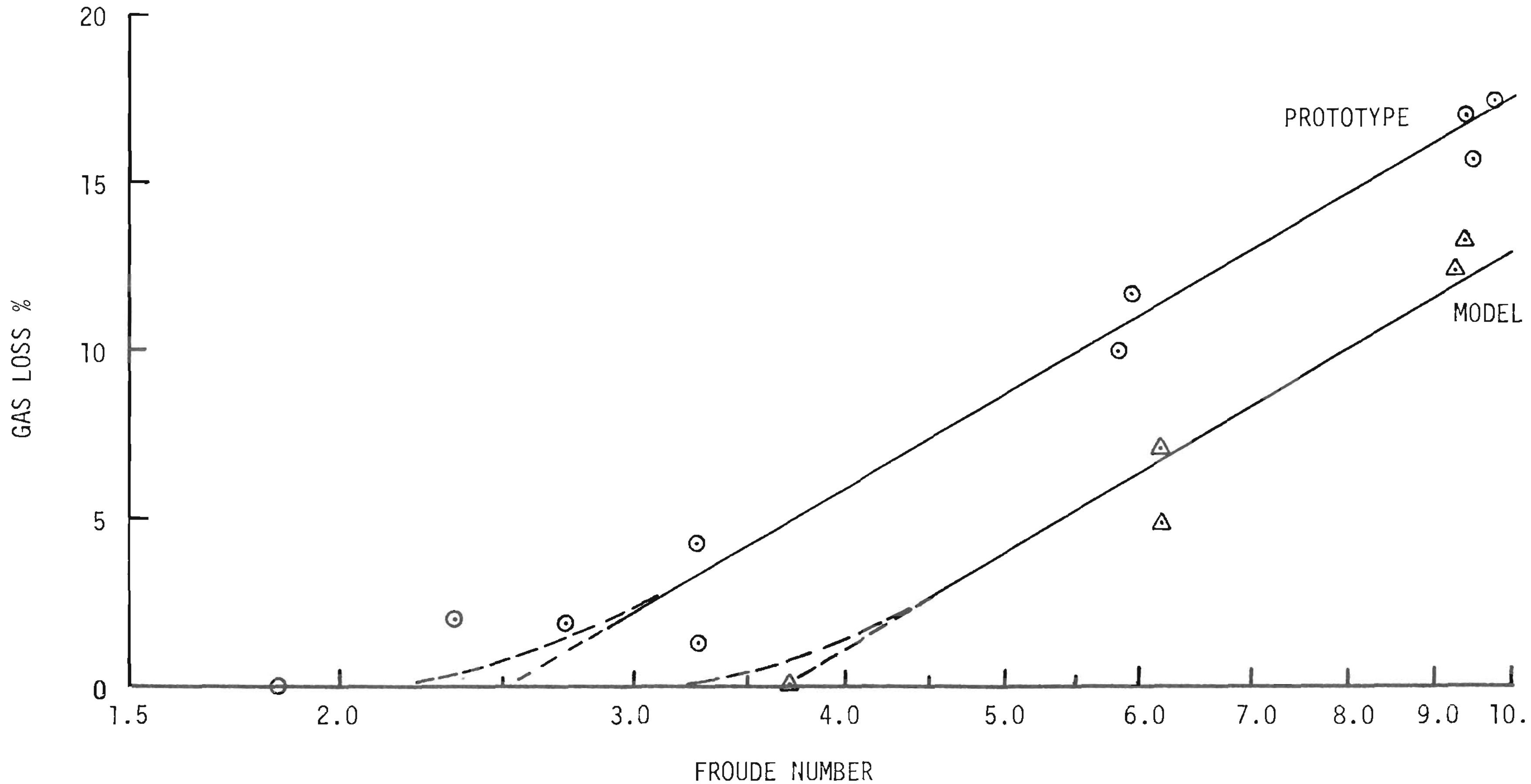

FIGURE 16: % GAS LOSS VERSUS FROUDE NUMBER

disregarded and the scaling criteria based on gas loss alone instead of the exchange coefficient.

49. Since the level of turbulence in the model was less than the level of turbulence in the prototype, the gas loss in the "model" was less than the gas loss in the "prototype". Figure 17 shows the ratio of gas loss in the model to gas loss in the prototype plotted against Froude Number. The gas losses used in the ratio computations were obtained from Figure 16. No simple relationship has been discernible to explain the relationship of model-to-prototype gas transfer.

PART VI: RECOMMENDATIONS

50. Further research should be conducted to examine in greater detail the relationship of gas loss and Froude number (Figure 16). This work should be performed with the "model" hydraulic jump sized between the "model" and "prototype" jumps already tested.

51. Tests with much greater discharge rates should be conducted. This would result in a much greater range in the Froudian scaling criterion for length. Jumps with higher Froude numbers ($F > 10$) should be tested to extend the range of the relationships already examined.

52. The two dimensionality of modeling the hydraulic jump should be verified (determine side-wall effects, if any). A much wider rectangular flume with unit discharges the same as those tested should be used to evaluate possible effects of the flume walls on the turbulence and, consequently, gas transfer.

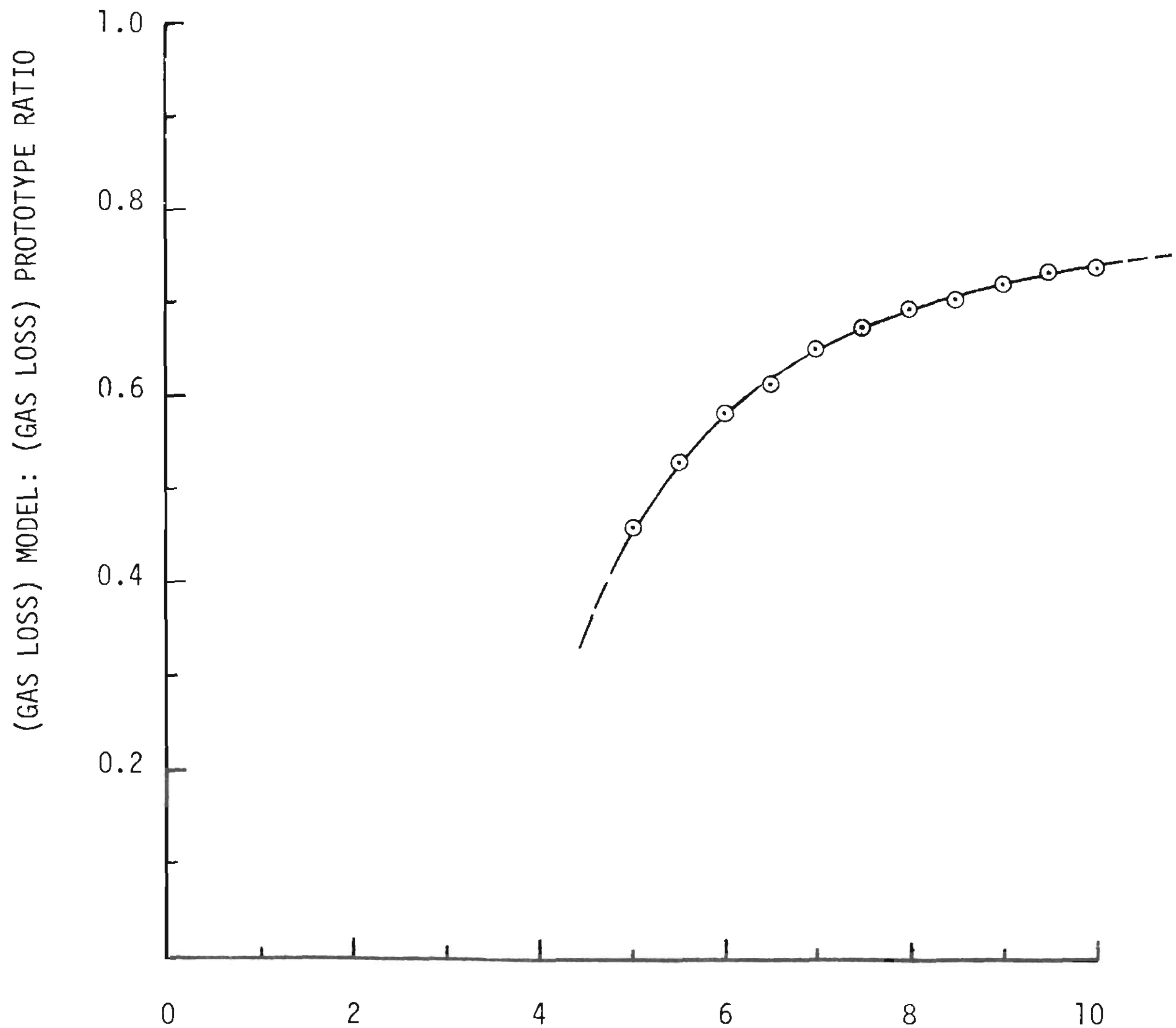

FIGURE 17: RATIO OF GAS LOSS IN MODEL VERSUS GAS LOSS IN PROTOTYPE

References

1. Tsivoglou, E. C., et. al., "Tracer Measurement of Atmospheric Reaeration: I. Laboratory Studies", WPCF Journal, Vol. 37, No. 10, Oct. 1965.

2. Tsivoglou, E. C., et. al., "Tracer Measurement of Stream Reaeration: II. Field Studies", WPCF Journal, Vol. 40, No. 2, Feb. 1968.

3. Tsivoglou, E. C. and Wallace, J. R., "Characterization of Stream Reaeration Capacity", EPA-R3-72-012, USEPA, 1972.

4. Rathbun, R. E., "Reaeration Coefficients of Streams - State-of-the-Art", ASCE Hyd. Div. Journal, Vol. 103, No. HY4, April 1977.

5. Chow, V. T., Open Channel Hydraulics, p. 395, McGraw-Hill, 1959.

6. Cohen, J. B., Setser, J. L., Kelley, W. D., and Shearer, S. D., "Analytical Method for the Determination of ^{3}H and ^{85}Kr in Aqueous Samples by Liquid Scintillation Techniques", Talanta, 1968.

7. Tsivoglou, E. C., "Tracer Measurement of Stream Reaeration," FWPCA, June 1967.

Appendix 1A

Observed Krypton-to-Dye Ratios and Pertinent Data for "Prototype" Hydraulic Jumps

Test 1

F = 9.5   V = 11.16 fps Y_1 = 0.043 ft   L = 3.40 ft

Station

	A	B	C	D
	104.7	84.10	89.70	86.00
	*	84.10	89.80	85.30
Ratio	*	67.80	87.40	87.80
	*	70.40	86.00	87.90
Mean:	104.7	76.60	88.23	86.75

Water Temperature: 23.9°C

From	To	Mean Time of Flow, sec
A	B	0.611
A	C	1.928
A	D	4.383

* Data not available or not taken

Test 2

F = 9.8   V = 11.38 fps Y_1 = 0.042 ft   L = 3.43 ft

Station

	A	B	C	D
	90.55	61.68	75.36	79.19
Ratio	95.57	57.78	76.00	76.28
	90.49	73.73	74.80	74.36
	91.79	71.60	77.74	79.95
Mean:	92.10	66.198	75.98	77.45

Water Temperature: 24.7°C

From	To	Mean Travel Time, sec
A	B	.53
A	C	1.62
A	D	3.96

Test 3

F = 9.4 V = 10.976 fps Y_1 = 0.042 ft L = 3.31 ft

Station

	A	B	C	D
	75.03	*	60.89	61.00
	74.18	*	61.59	61.26
Ratio	*	*	62.59	59.84
	*	*	62.53	62.36
Mean:	74.61		61.90	61.12

Water Temperature: 23.15°C

From	To	Mean Travel Time, sec
A	B	0.70
A	C	1.29
A	D	2.87

* Data not available or not taken

Test 4

F = 5.95 V = 8.09 fps Y_1 = 0.057 ft L = 2.76 ft

Station

	A	B	C	D
	91.09	79.70	80.21	80.51
	92.11	82.72	80.49	80.65
Ratio	91.73	*	82.89	83.35
	92.85	*	81.82	83.14
Mean:	91.95	81.21	81.36	81.91

Water Temperature: 23.2°C

From	To	Mean Travel Time, sec
A	B	1.37
A	C	2.80
A	D	5.84

* Data not available or not taken

Test 5

F = 5.85 V = 7.856 fps Y_1 = 0.056 L = 2.68

Station

	A	B	C	D
	79.61	73.28	74.11	72.71
	80.60	73.61	74.82	72.53
Ratio	80.31	71.54	72.55	71.83
	83.35	72.94	71.72	
Mean:	80.97	72.85	73.30	72.35

Water Temperature: 23.15°C

From	To	Mean Travel Time, t, sec
A	B	1.32
A	C	3.70
A	D	5.82

Test 6

F = 3.27 V = 5.38 fps Y_1 = 0.084 ft L = 1.90 ft

Station

	A	B	C	D
	96.54	90.46	93.46	92.79
	94.43	91.09	91.54	92.01
Ratio	97.04	92.62	93.31	90.61
	97.64	94.88	93.90	91.61
Mean:	96.42	92.26	93.06	91.76

Water Temperature: 23.4°C

From	To	Mean Travel Time, t, sec
A	B	0.95
A	C	1.96
A	D	3.57

Test 7

F = 3.28 V = 5.43 fps Y_1 = 0.085 ft L = 1.93 ft

Station

	A	B	C	D
	91.64	90.92	*	93.11
	95.64	93.16	*	93.09
Ratio	93.47	92.82	*	92.19
	93.12	91.92	*	90.54
Mean:	93.47	92.21		92.23

Water Temperature: 23.0°C

From	To	Mean Travel Time, t, sec
A	B	0.99
A	C	*
A	D	4.17

* Data not available or not taken

Test 8

F = 2.72 V = 4.83 fps Y_1 = 0.0978 ft L = 1.68 ft

Station

	A	B	C	D
	94.72	95.36	91.39	92.07
	95.15	*	91.64	89.12
Ratio	96.13	92.63	93.26	92.54
	95.34	92.85	90.52	93.22
Mean:	95.33	93.61	91.70	91.74

Water Temperature: 23.4°C

From	To	Mean Travel Time, t, sec
A	B	0.94
A	C	2.25
A	D	3.57

* Data not available or not taken

Test 9

F = 2.34   V = 4.34 fps Y_1 = 0.107 ft   L = 1.41 ft

	Station A	Station B	Station C	Station D
	87.75	84.51	81.81	86.37
	89.06	85.99	84.19	83.16
Ratio	86.07	84.80	86.97	83.20
	84.46	85.03	86.52	84.94
Mean:	86.83	85.08	84.87	84.42

Water Temperature: 23.4°C

From	To	Mean Travel Time, t, sec
A	B	0.71
A	C	1.42
A	D	2.61

Test 10

F = 1.84   V = 3.66 fps Y_1 = 0.123 ft   L = 1.11 ft

	Station A	Station B	Station C	Station D
	19.46	19.57	20.14	20.09
	19.71	19.34	19.63	19.67
Ratio	*	19.54	19.60	19.89
	*	*	19.24	18.37
Mean:	19.59	19.48	19.65	19.51

Water Temperature: 22.8°C

From	To	Mean Travel Time, t, sec
A	B	0.47
A	C	0.99
A	D	1.48

* Data not available or not taken

Appendix 1B

Krypton-to-Dye Ratios for "Model" Hydraulic Jumps

Test 1

$F = 9.30$ $V = 8.867$ fps $Y_1 = 0.0282$ ft $L = 2.19$ ft

Station

	A	B	C	D
	112.03	99.75	96.29	98.81
	112.64	97.49	96.75	99.14
Ratio	110.48	94.01	97.21	96.67
	110.95	99.47	97.03	97.74
Mean:	111.52	97.68	96.82	98.09

Water Temperature: 22.2°C

From	To	Mean Travel Time, t, sec
A	B	1.65
A	C	4.31
A	D	8.09

Test 2

$F = 9.4$ $V = 9.12$ fps $Y_1 = 0.029$ ft $L = 2.27$ ft

Station

	A	B	C	D
	112.04	99.09	98.82	96.12
	115.95	98.15	98.05	94.89
Ratio	*	98.29	97.65	96.00
	112.98	99.18	99.31	96.14
Mean:	113.66	98.68	98.46	95.79

Water Temperature: 22.2°C

From	To	Mean Travel Time, t, sec
A	B	1.51
A	C	3.76
A	D	8.22

* Data not available or not taken

Test 3

$F = 6.2$ $V = 6.86$ fps $Y_1 = 0.0384$ ft $L = 1.93$ ft

Station

	A	B	C	D
	89.79	84.75	84.43	*
	88.61	85.25	83.61	*
Ratio	88.53	82.76	83.88	*
	89.24	85.78	84.28	*
Mean:	89.04	84.64	84.05	

Water Temperature: 22.2°C

From	To	Mean Travel Time, t, sec
A	B	1.49
A	C	3.86
A	D	*

* Data not available or not taken

Test 4

$F = 6.19$ $V = 6.86$ fps $Y_1 = 0.0381$ ft $L = 1.92$ ft

Station

	A	B	C	D
	92.41	87.28	87.72	*
	95.58	88.42	87.63	*
Ratio	*	86.32	88.87	*
	92.02	88.55	88.39	*
Mean:	94.34	87.64	88.15	

Water Temperature: 22.1°C

From	To	Mean Travel Time, t, sec
A	B	1.46
A	C	3.83
A	D	*

* Data not available or not taken

Test 5

$F = 3.7$ $V = 4.88$ fps $Y_1 = 0.054$ ft $L = 1.46$ ft

Station

	A	B	C	D
	89.95	89.70	86.64	*
	87.61	91.61	89.10	*
Ratio	89.77	89.22	85.66	*
	92.44	89.94	85.35	*
Mean:	89.94	90.12	86.69	

Water Temperature: 22.2°C

From	To	Mean Travel Time, t, sec
A	B	1.00
A	C	2.11
A	D	*

* Data not available or not taken

Appendix 2A

Krypton-to-Dye Ratios Versus Time Prototype Tests

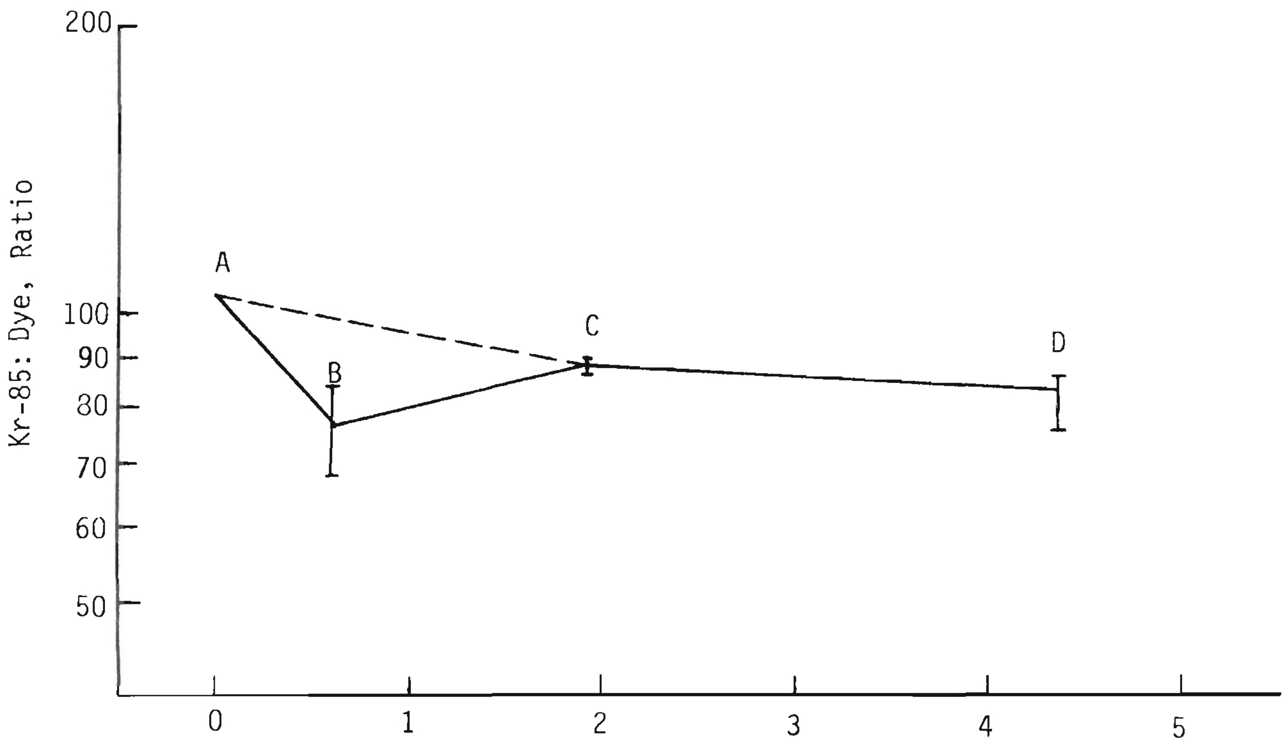

TIME, SECONDS, ARBITRARY ZERO

TEST #1, F = 9.50, PROTOTYPE JUMP

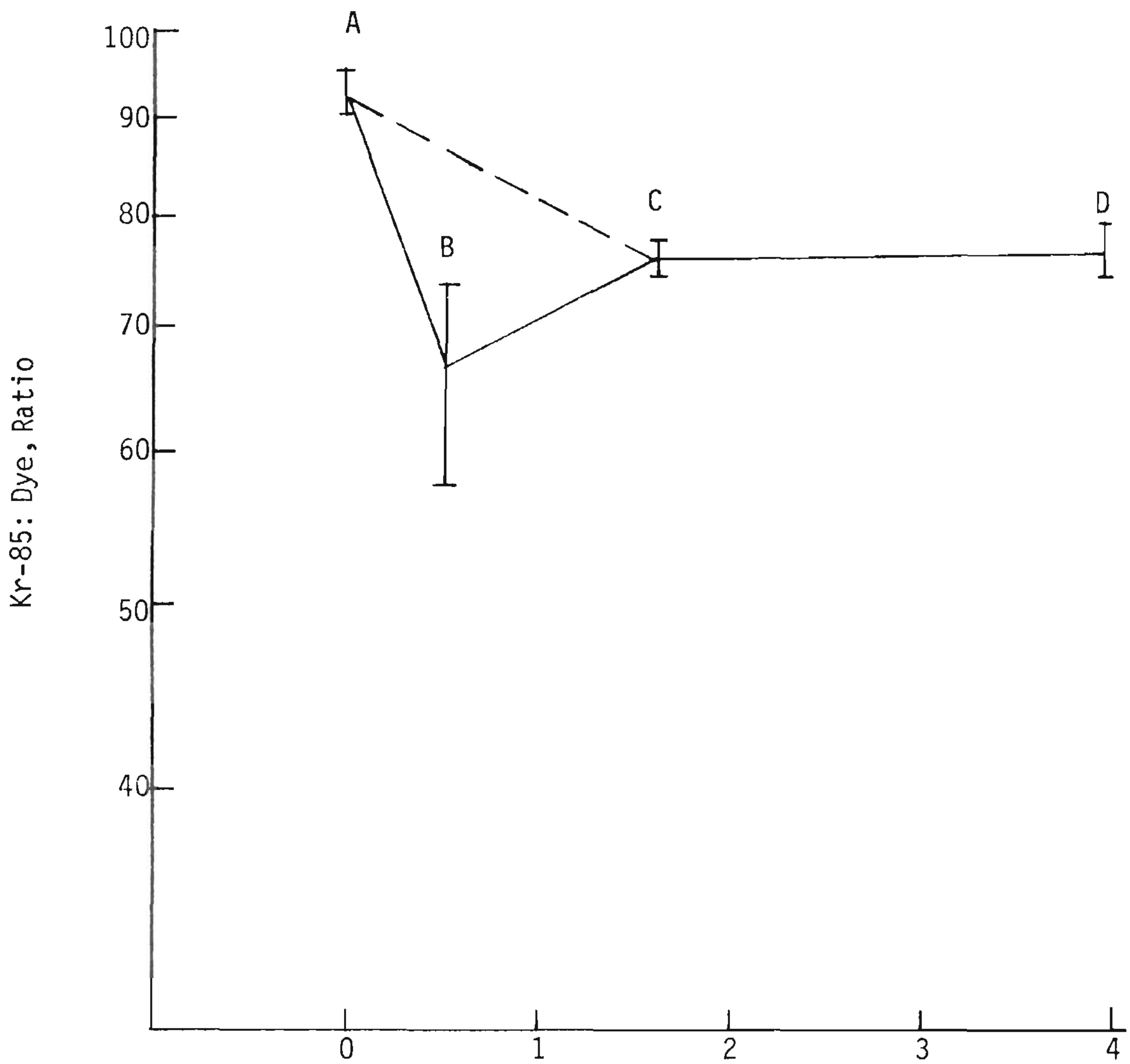

TIME, SECONDS, ARBITRARY ZERO

TEST #2, F = 9.80, PROTOTYPE JUMP

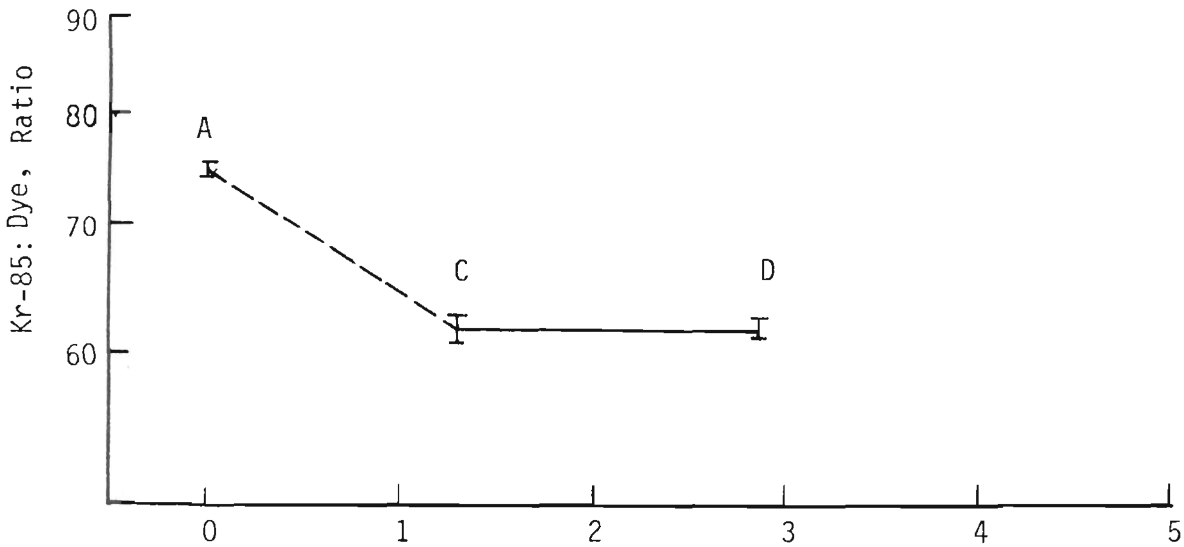

TIME, SECONDS, ARBITRARY ZERO

TEST #3, F = 9.40, PROTOTYPE JUMP

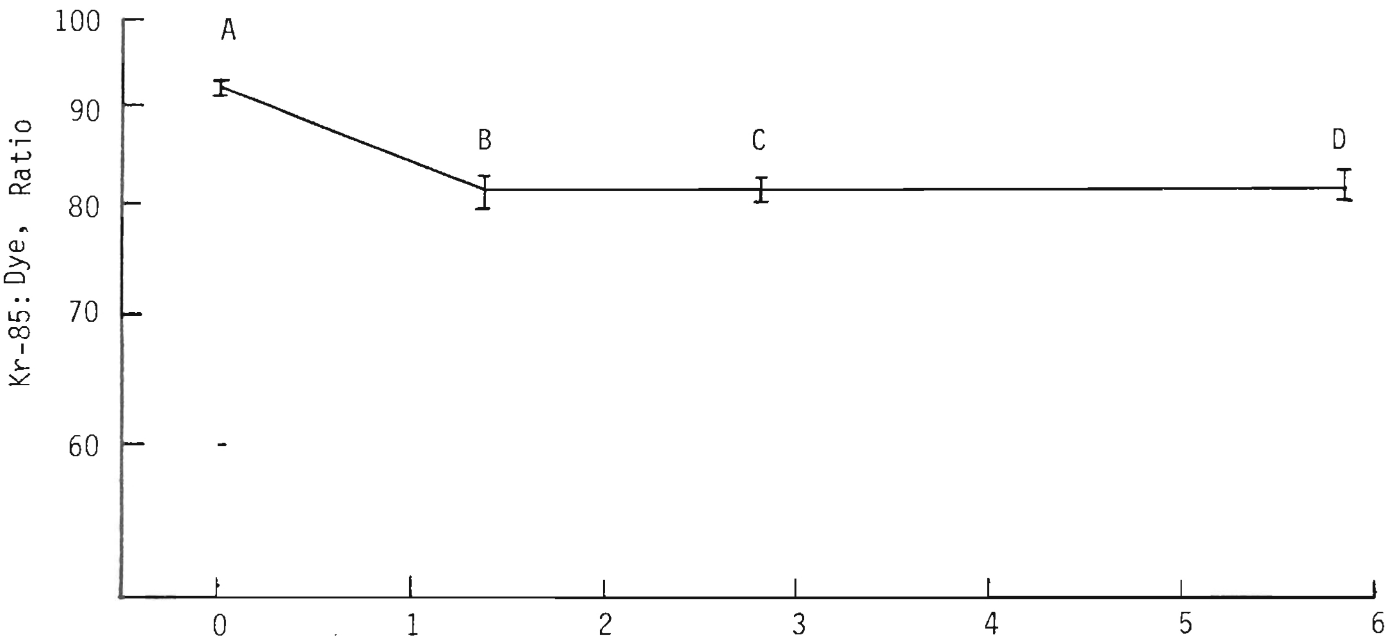

TIME, SECONDS, ARBITRARY ZERO

TEST #4, F = 5.95, PROTOTYPE JUMP

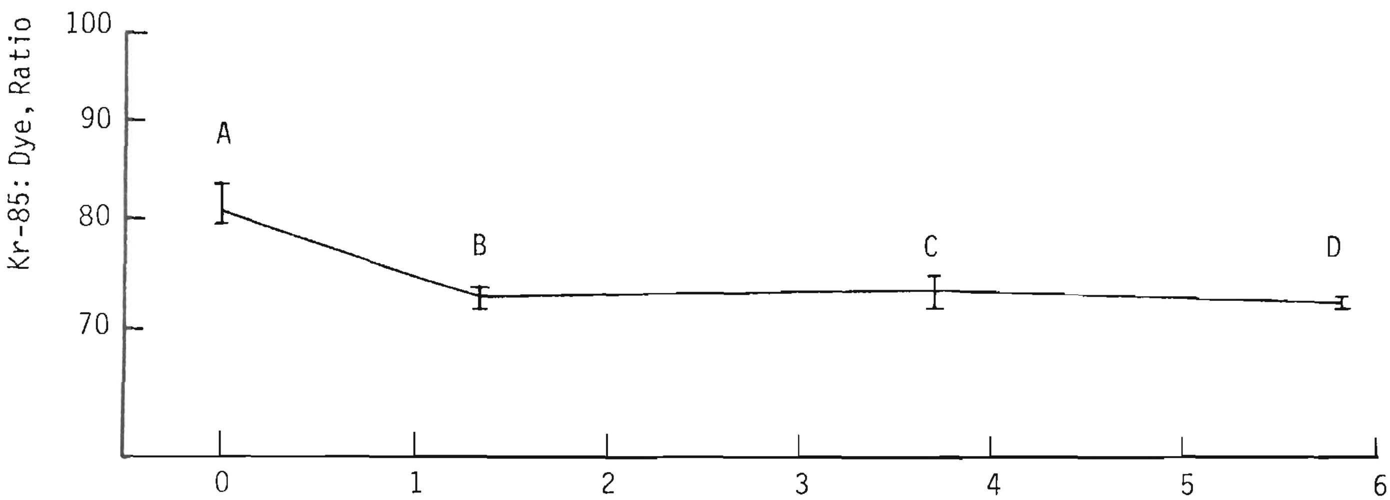

TIME, SECONDS, ARBITRARY ZERO

TEST #5, F = 5.85, PROTOTYPE JUMP

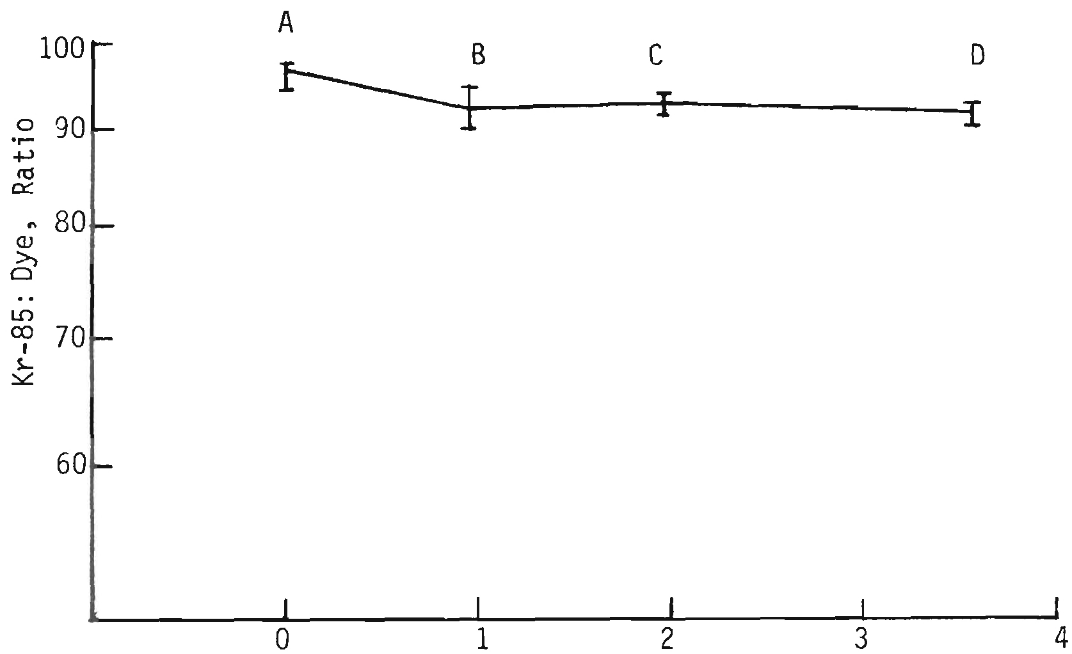

TIME, SECONDS, ARBITRARY ZERO

TEST #6, F = 3.27, PROTOTYPE JUMP

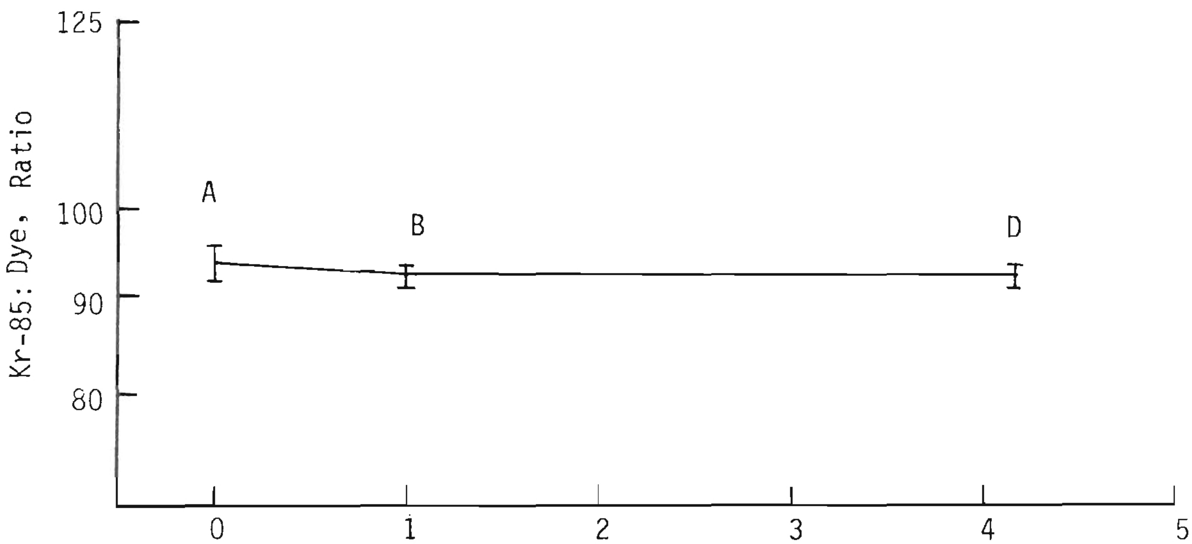

TIME, SECONDS, ARBITRARY ZERO

TEST #7, F = 3.28, PROTOTYPE JUMP

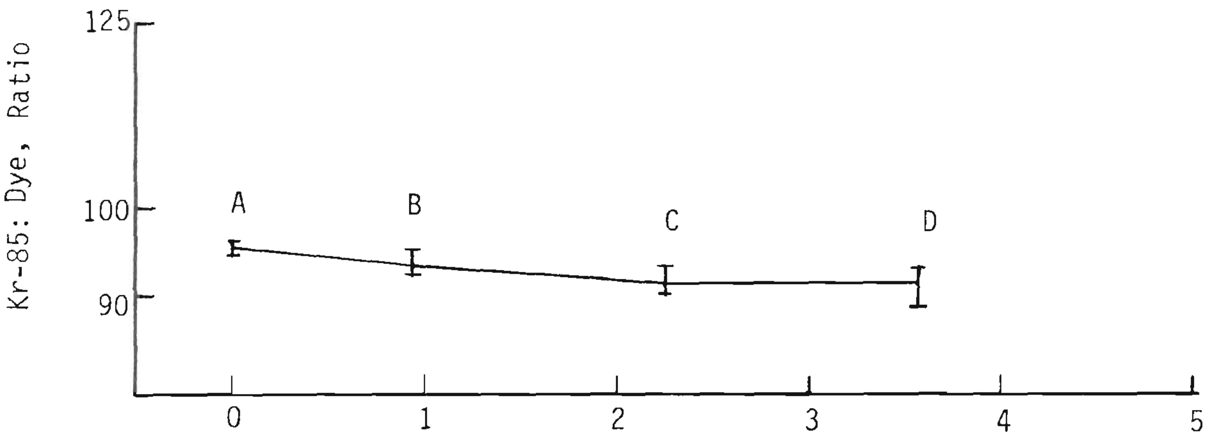

TIME, SECONDS, ARBITRARY ZERO

TEST #8, F = 2.72, PROTOTYPE JUMP

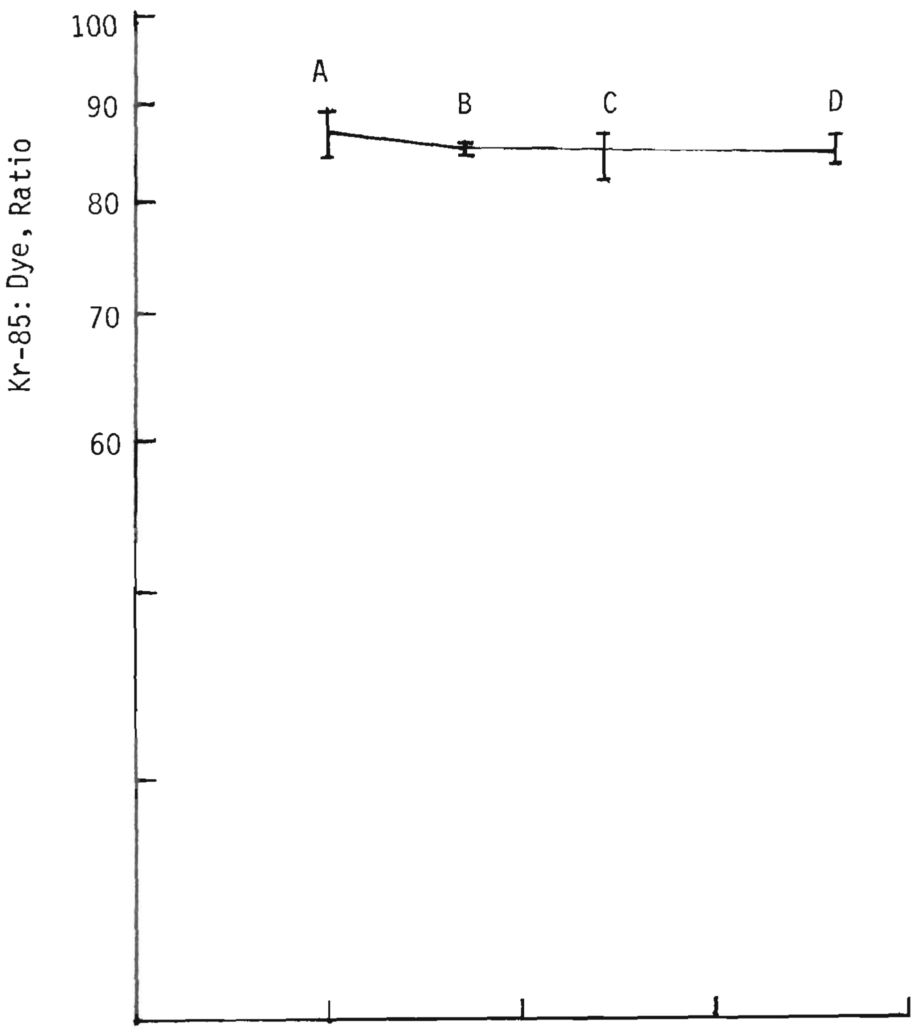

TIME, SECONDS, ARBITRARY ZERO

TEST #9, F = 2.34, PROTOTYPE JUMP

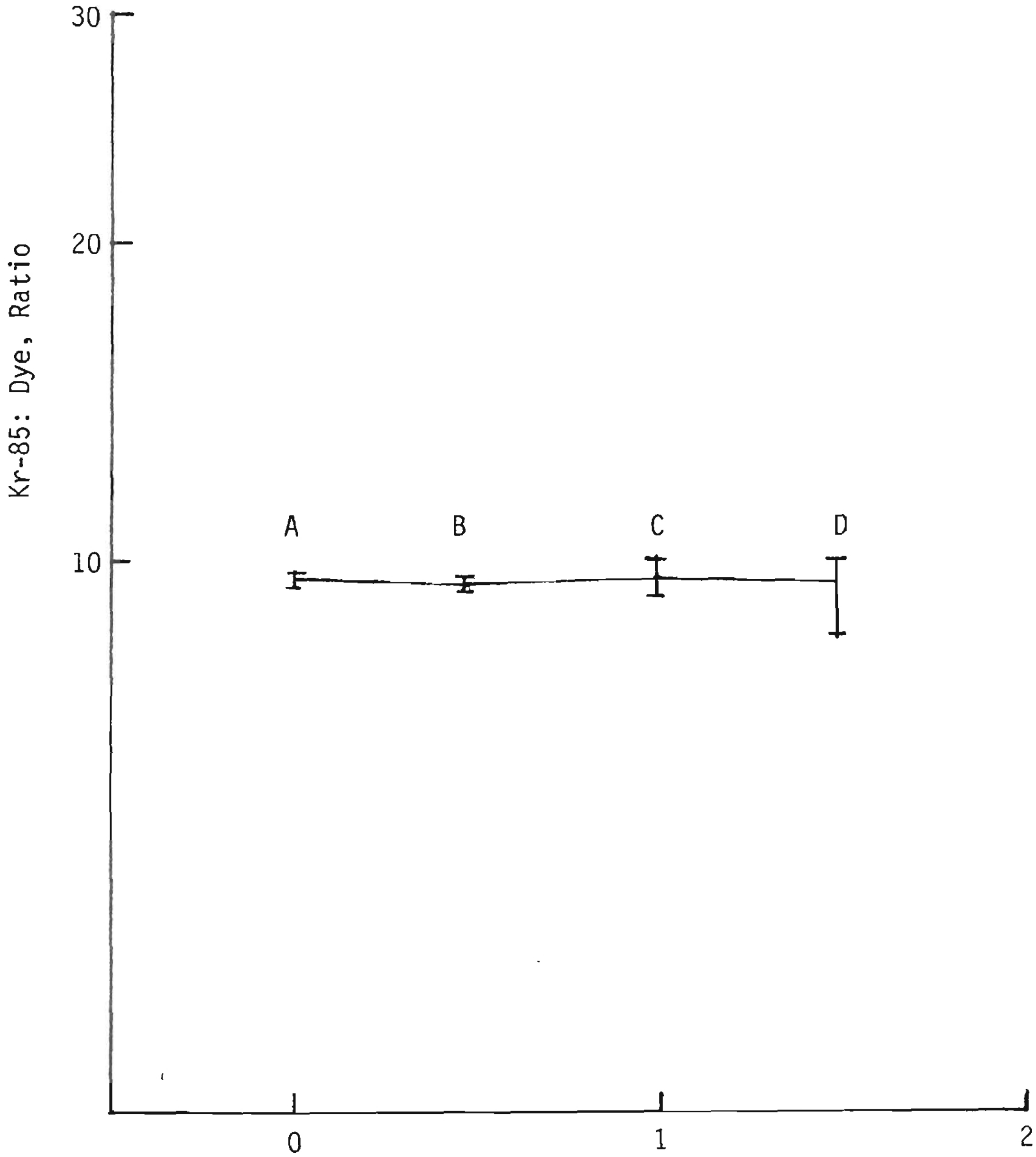

TIME, SECONDS, ARBITRARY ZERO

TEST #10, F = 1.84, PROTOTYPE JUMP

Appendix 2B

Krypton-to-Dye Ratios Versus Time Model Tests

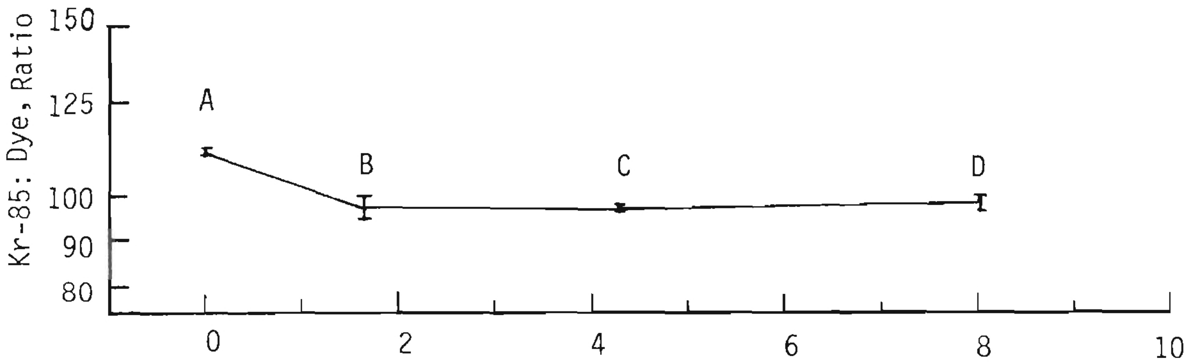

TIME, SECONDS, ARBITRARY ZERO

TEST #1, F = 9.30, MODEL JUMP

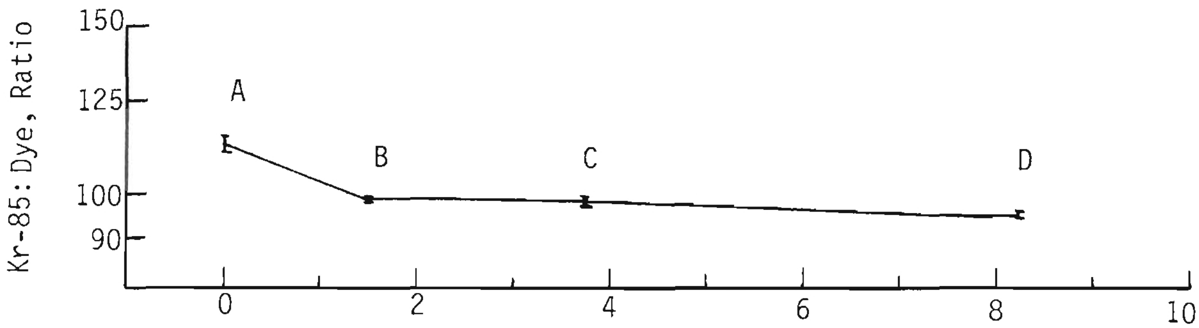

TIME, SECONDS, ARBITRARY ZERO

TEST #2, F = 9.40, MODEL JUMP

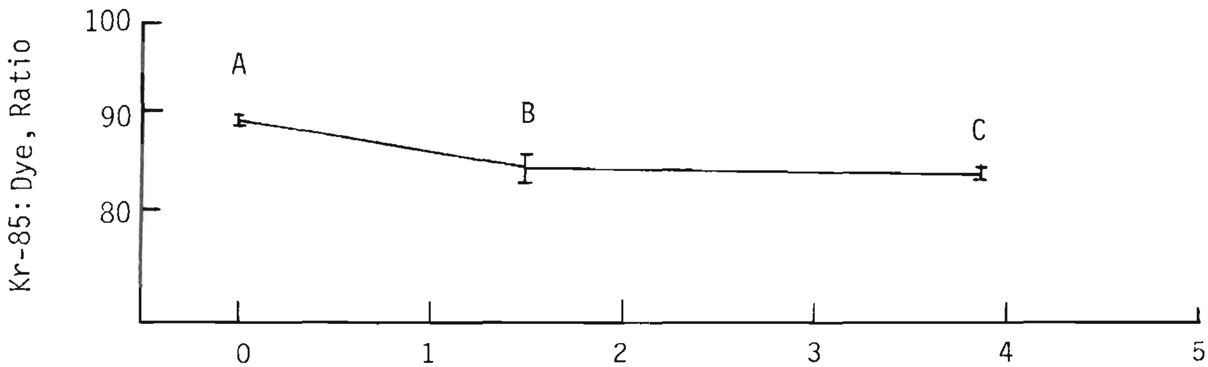

TIME, SECONDS, ARBITRARY ZERO

TEST #3, F = 6.2, MODEL JUMP

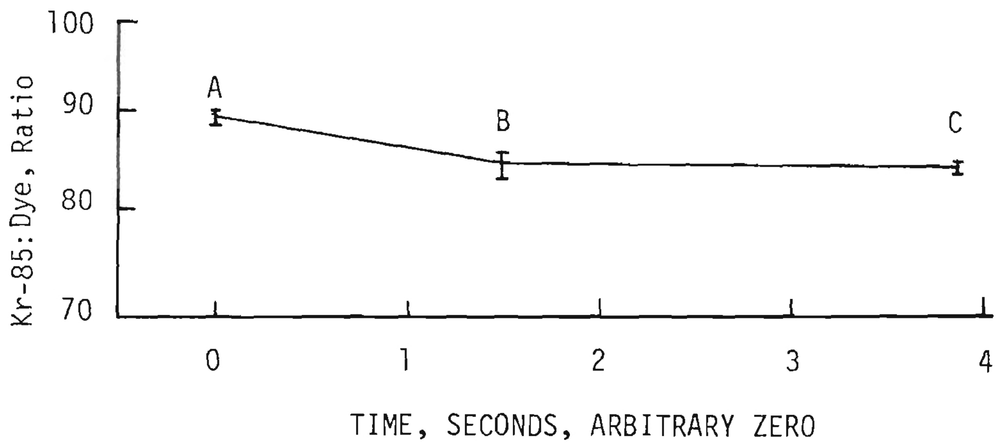

TEST #4, F = 6.2 MODEL JUMP

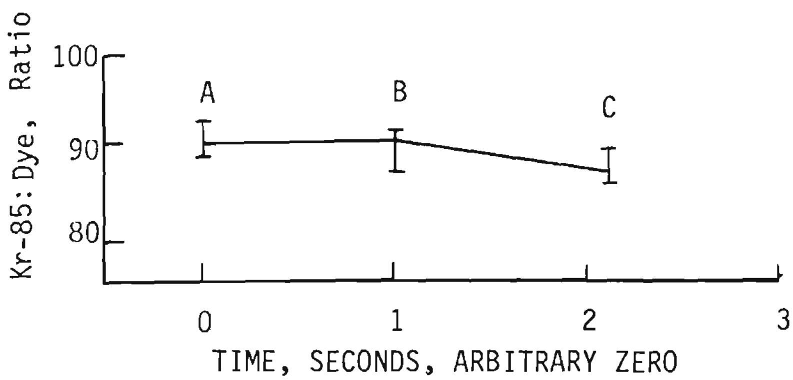

TEST #5, F = 3.7, MODEL JUMP